

LETTER

Macroscopic electrostatic effects in ATR-FTIR spectra of modern and archeological bones[‡]

JULIE AUFORT^{1,*}, MATTHIEU LEBON², XAVIER GALLET², LOÏC SÉGALEN³, CHRISTEL GERVAIS⁴,
CHRISTIAN BROUDER¹, AND ÉTIENNE BALAN¹

¹IMPMC, Sorbonne Université, UMR CNRS 7590, UMR IRD 206, MNHN, 4 place Jussieu, 75252 Paris, cedex 05 France

²HNHP, Sorbonne Université, UMR CNRS 7194, MNHN, Université Perpignan Via Domitia, 17 Place du Trocadéro, 75116 Paris, France

³ISTEP, Sorbonne Université, UMR CNRS 7193, 4 place Jussieu, 75252 Paris, cedex 05 France

⁴LCMCP, Sorbonne Université, UMR CNRS 7574, 4 place Jussieu, 75252 Paris, cedex 05, France

ABSTRACT

Bones mostly consist of composite materials based on almost equivalent volume fractions of mineral (apatite) and organic (collagen) components. Accordingly, their infrared spectroscopic properties should reflect this composite nature. In this letter, we show by theory and experiment that the variability of the strong phosphate bands in the ATR-FTIR spectra of a series of modern and archeological bone samples can be related to electrostatic interactions affecting apatite particles and depending on the bone collagen content. Key parameters controlling the shape of these bands are the mineral volume fraction and the dielectric constant of the embedding matrix. The magnitude of these effects is larger than the one related to microscopic changes of the apatite structure. Consequently, the interplay of microscopic and macroscopic parameters should be considered when using FTIR spectroscopy to monitor the preservation state of bioapatite during diagenetic and fossilization processes, especially during the degradation of the organic fraction of bone.

Keywords: ATR-FTIR spectroscopy, bone, fossilization, electrostatic properties; Biomaterials—Mineralogy Meets Medicine

INTRODUCTION

Vertebrate skeletons mostly consist of composite materials containing a mineral component and a fraction of organic and water molecules (Pasteris et al. 2008). The inorganic component is usually described as nanocrystalline carbonate-bearing hydroxylapatite [$\text{Ca}_5(\text{PO}_4)_3\text{OH}$], although more complex structures and chemical compositions have been observed (e.g., Pasteris et al. 2008; Li and Pasteris 2014). Bones consist of about 50 vol% of ~2 nm thick, 10–20 nm wide, and 20–50 nm long apatitic nanocrystallites and a near equivalent volume of collagen fibrils (Glimcher 2006; Pasteris et al. 2008). Compared to bone, tooth enamel lacks collagen, contains ~1–2 vol% of organic compounds and about 2 vol% of water, and displays larger apatite crystallites making up for ~90 vol% of the material (LeGeros and LeGeros 1984; Elliott 2002; Skinner 2005).

Key information on the atomic-scale organization of such complex materials is provided by spectroscopic methods (e.g., Pasteris et al. 2008; Yi et al. 2014). As it is a versatile technique requiring only small sample amounts, Fourier-transform infrared (FTIR) spectroscopy has been widely applied to the study of bones and teeth. Although most of these studies have biomedical goals, FTIR spectroscopy also allows efficient screening of the preservation state of skeleton remains prior to isotopic and chemical analysis for paleo-environmental reconstructions or radiocarbon dating (e.g.; Trueman et al. 2008; Roche et al. 2010;

Lebon et al. 2016; Snoeck and Pellegrini 2015). Diagenetic transformation of bones and teeth following burial often leads to an increase in crystallinity as well as a decrease in organic fraction and structural carbonate contents (e.g., Hedges 2002; Trueman et al. 2008).

In practice, FTIR spectra of bioapatite are increasingly recorded in the attenuated total reflection (ATR) mode (e.g., Stathopoulou et al. 2008; Thompson et al. 2009; Lebon et al. 2016; Beasley et al. 2014; Surmik et al. 2016). Unlike conventional transmission geometry, ATR spectroscopy does not require the multistep preparation of dry and homogeneous pellets containing a percent-level fraction of solid particles dispersed in a KBr matrix. The absorption-like ATR spectrum is recorded on the packed sample powder by measuring its reflection coefficient at the interface with a highly refractive material. However, the different geometry and nature of the sample may impede a straightforward comparison of ATR with transmission spectra (Aufort et al. 2016). Differences in the crystallinity degree and carbonate-to-phosphate ratio of samples measured in transmission, ATR, and diffuse reflectance geometries have been reported (Beasley et al. 2014). The position and intensity of the ATR signal also depend on the refractive index of the ATR crystal (Boulet-Audet et al. 2010), typically diamond ($n = 2.4$) or germanium ($n = 4$). Use of Ge usually requires larger amounts of sample and leads to a comparatively smaller band intensity, thus limiting the detection of relatively weak bands, such as those related to carbonate impurities and organic matter. In addition, the ATR spectra depend on characteristics of the sample microstructure, such as porosity, nature of the embedding medium, aggregation state, and shape of particles, as recently shown for apatite (Aufort

* E-mail: Julie.Aufort@upmc.fr

† Special collection papers can be found online at <http://www.minsocam.org/MSA/AmMin/special-collections.html>.

‡ Open access: Article available to all readers online. This article is CC-BY-NC-ND.

et al. 2016). This dependence arises from the long-range electrostatic interactions within and between particles, interactions that also affect the transmission spectra (e.g., Iglesias et al. 1990; Balan et al. 2011; Kendrick and Burnett 2016).

Based on these observations, it can be anticipated that the FTIR spectra of composite biomaterials such as bone should depend on the relative fractions of mineral and organic constituents through macroscopic electrostatic interactions. In this contribution, we show that the line-shape variability of the ATR-FTIR spectrum of modern and archaeological bones can be accounted for by combining the description of the intrinsic vibrational properties of the mineral component with an electrostatic model taking into consideration their variable collagen fraction.

MATERIALS AND METHODS

Three archaeological animal bone and a modern ox bone samples (Table 1), previously investigated using ATR-FTIR spectroscopy by Lebon et al. (2016), were chosen for their various states of collagen preservation as well as a modern tooth enamel sample previously investigated by Yi et al. (2014). For each sample, about 50 mg of powder were finely ground with agate mortar and pestle. The ATR-FTIR spectra were recorded using a Quest ATR device (Specac) and a Nicolet 6700 FTIR spectrometer. Pure powder samples were packed at the surface of the ATR crystal and spectra recorded between 400 and 4000 cm^{-1} by averaging 100 scans with a resolution of 1 cm^{-1} . For each sample, two different spectra were recorded on the same Quest ATR device using interchangeable diamond and germanium ATR crystals. The raw ATR spectra are reported in absorbance units, without any correction treatment or baseline subtraction.

The modeling strategy has been extensively detailed in Aufort et al. (2016). Briefly, the theoretical ATR spectrum is obtained by computing the frequency-dependent reflection coefficient with a 45° incidence angle at the interface between the ATR crystal, defined as a homogeneous isotropic medium with constant refractive index (2.4 for diamond and 4 for Ge), and the sample. The powder sample is characterized by a dielectric function computed for a mixture of spherical apatite particles and embedding matrix, using the Bruggeman effective medium model (Bruggeman 1935). In this model, both the particles and matrix domains are considered as being inserted in an effective medium, leading to a self-consistent relation between the effective medium properties and those of individual constituents. The uniaxial dielectric tensor of bulk apatite is obtained from its microscopic vibrational and dielectric properties using a Drude-Lorentz expression (Table 2). All microscopic sources of broadening are assumed to be effectively accounted for by the damping parameter of the Drude-Lorentz model. The embedding matrix is described using a constant refractive index varying between 1 for air in a porous mineral-air sample to ~ 1.6 for pure collagen (Wang et al. 1996). No attempt was made to consider the specific vibrational properties of collagen. The varying parameters used to calculate the theoretical spectra are thus restricted to the refractive index of the ATR crystal, the mineral fraction and the dielectric constant of the embedding matrix (ϵ_b) (Table 1). Theoretical spectra computed for systematic variations of these parameters are reported as Supplemental Information. The effective medium approximation considers the sample homogeneous at the length scale of the experiment, typically requiring particle sizes smaller than a few micrometers. To compare calculation with experiment, the theoretical intensities were multiplied by a scale factor, to account for inhomogeneities of the samples at larger length scales, e.g., related to the imperfect grinding of organic-mineral mixtures and/or imperfect contact between the powder sample and the ATR crystal (Table 1).

RESULTS AND DISCUSSION

Experimental diamond and Ge ATR spectra of modern ox bone (Fig. 1) display the usual absorption bands ascribed to the internal vibrations of apatitic orthophosphate groups, to structural carbonate impurities located at the A and B sites (hydroxyl and phosphate sites, respectively) of apatite structure, as well as to the amide bands related to the collagen matrix (e.g., Elliott 2002). Its collagen content is estimated to be ~ 23 wt% as assessed from nitrogen concentration and intensity of amide bands (Lebon et al. 2016). A weak and broad feature at ~ 700 cm^{-1}

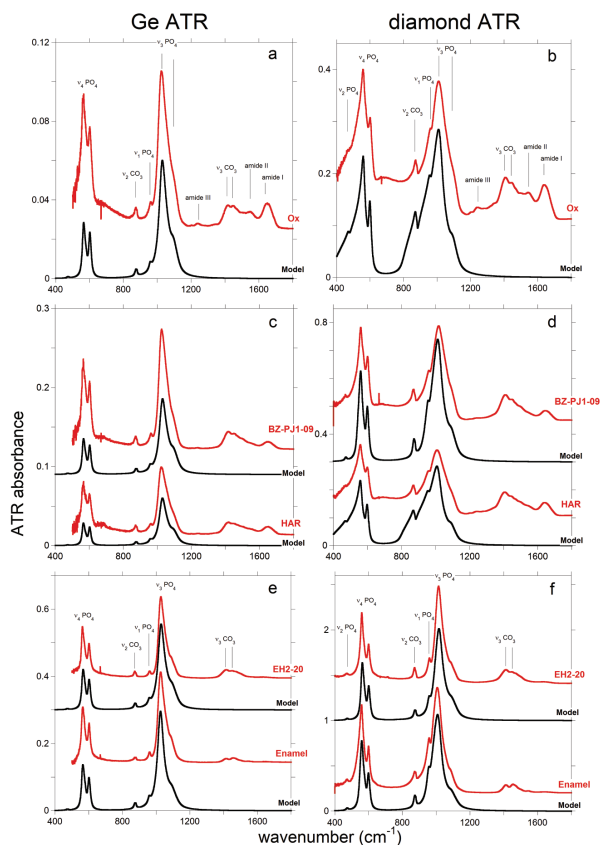


FIGURE 1. Experimental and modelled ATR-FTIR spectra of modern ox bones (a, b), archaeological animal bones with intermediate levels of collagen preservation (c, d); low collagen containing archaeological bone and tooth enamel (e, f). Spectra a, c, and e have been recorded using a Ge ATR crystal. Spectra b, d, and f have been recorded using a diamond ATR crystal. Experimental ATR-FTIR spectra have been shifted vertically for comparison.

is related to collagen absorption (Supplemental Information). Similar spectral features for the phosphate, carbonate, and amide bands are observed in archaeological bones HAR and BZ-PJ1-09 that still display a significant collagen content (16 and 11 wt%, respectively). The spectrum of altered archaeological bone (EH2-20) and modern tooth enamel display similar absorption bands except that the collagen amide bands are absent. The ATR spectra of these two samples are about four times more intense than those recorded on the collagen-rich bone samples. As previously observed by Aufort et al. (2016), significant differences are observed between the spectra recorded using a Ge or a diamond crystal for the whole series of samples. Beside a stronger intensity, the intense ν_3 stretching and ν_4 bending PO_4 bands of the diamond-ATR spectra are broadened on their low-frequency side, and the ν_3 band overlaps with the weaker $\nu_1 \text{PO}_4$ and $\nu_2 \text{CO}_3$ bands. They also display a greater variability among the samples, their low-frequency asymmetry being more pronounced for the collagen-rich samples (Fig. 1). In contrast, the variability of the Ge spectra is weaker and mostly related to variations in the relative intensities of the amide and structural carbonate bands. Thus, the presence of the collagen matrix

TABLE 1. Sample source and description, N wt%, and parameters used to define the binary composite for the corresponding modeled ATR spectra shown in Figure 1

Sample	Description, origin	Age	N, wt% ^a	Min. fraction vol%	ϵ_{host}	Scale factor
Ox	Ox bone	Modern	3.96 ^a	40	2.5	0.175
HAR	Harsova Tell, Romania	Chalcolithic	2.75 ^a	40	2.5	0.175
BZ-PJ1-09	Bize-Tournal Cave, France	Paleolithic	1.80 ^a	40	1.9	0.33
EH2-20	El Harroura Cave, Morocco	Neolithic	0.16 ^a	45	1.0	1.0
Enamel	Camelidae tooth enamel ^b	Modern	n.d.	55	1.0	0.8

^a Lebon et al. (2016), ^b Yi et al. (2014).

affects the intense phosphate bands of the diamond ATR spectra of bone samples but the similarities of Ge-ATR spectra suggest that this effect is not associated with a strong modification of the microscopic structure of apatitic crystallites.

Based on a systematic analysis of spectral changes related to variations of the macroscopic parameters describing the composite nature of the samples (Supplemental¹ Information), further insight in the observed variations can be gained from the comparison of experimental and modeled spectra. We stress that our modeling strategy involves a compromise between a minimal variation of model parameters (Table 1) and a reproduction of relative variations observed among the spectra. The bulk apatite properties (Table 2) are modeled using frequencies and force oscillator strengths close to those previously used to model fluorapatite spectra (Aufort et al. 2016). However, significantly higher broadening parameters must be used to account for the lower degree of crystalline order and higher strain of biogenic apatite particles. The ν_2 CO₃ bands that can overlap with phosphate-related bands of apatite have also been introduced in the model. The B-type resonance corresponds to substitution of CO₃ for PO₄, presumably occupying a triangular face of the tetrahedral phosphate sites, and has been assumed to be isotropic. Its broadening parameter is similar to that used for ν_4 and ν_1 PO₄ bands. The A-type bands correspond to carbonate groups occupying channel sites with an orientation parallel to the *c*-axis. A comparatively smaller broadening parameter was found to account for the shape of the A-type band, suggesting that the local environment of channel carbonates is less sensitive to variations in the apatite structural order. The stretching CO₃ and amide bands observed at higher frequencies (Fig. 1) have not been included in the models as they do not overlap with the apatite-related phosphate bands. A single set of parameters (Table 2) describing the microscopic properties of bulk apatite is used to model the ATR spectra of the whole sample series. Each sample is thus considered as a binary composite defined by three parameters (Table 1): the mineral fraction, the dielectric constant of the other component, and a scale factor. The Ge and diamond ATR spectra are then computed by only varying the refractive index of the ATR crystal.

Collagen-poor enamel and EH2-20 bone samples are well-described as an apatite/air composite, with a larger mineral fraction for enamel than for the heavily transformed archeological bone (55% vs. 45%). These samples require almost no scaling of theoretical intensities to match the experimental ones (Table 1). When comparing the diamond and Ge spectra, the model reproduces the stronger spectral intensity and the downshift of ν_4 and ν_3 PO₄ bands observed in the diamond spectrum. Although

TABLE 2. Parameters used to model the dielectric tensor of carbonated hydroxylapatite

Symmetry	Mode	ω_i (cm ⁻¹)	$A_{i,\alpha}$ (cm ⁻¹)	Γ_i (cm ⁻¹)
(z)	ν_3 (PO ₄)	1027	665	40
	ν_2 (CO ₃) B	874	80	16
	ν_4 (PO ₄)	560	300	15
(x,y)	ν_2 (PO ₄)	473	45	15
	ν_3 (PO ₄)	1090	270	40
	ν_3 (PO ₄)	1032	630	40
	ν_1 (PO ₄)	958	110	18
	ν_2 (CO ₃) A	880	30	5
	ν_2 (CO ₃) B	874	80	16
	ν_4 (PO ₄)	600	215	15
	ν_4 (PO ₄)	580	120	15

Notes: The Cartesian components of the uniaxial tensor are defined by a Drude-Lorentz expression:

$$\epsilon_{\alpha}(\omega) = \epsilon_{\infty} + \sum_i \frac{A_{i,\alpha}^2}{(\omega_i^2 - \omega^2 - i\omega\Gamma_i)}$$

where α refers to the Cartesian axis, $\epsilon_{\infty} = 2.65$ is the high-frequency dielectric contribution considered here to be real, constant, and isotropic, ω_i is the vibrational transverse optical frequency, $A_{i,\alpha}^2$ the effective mode oscillator strength, and Γ_i is the damping parameter of vibrational mode *i*.

the maximum of the ν_3 PO₄ bands was observed at 1026 cm⁻¹ in the Ge spectrum, close to the corresponding transverse optical frequencies (1027 and 1032 cm⁻¹; Table 2), it is shifted to 1014 and 1006 cm⁻¹ in the diamond-ATR spectrum of the EH2-20 and modern enamel samples. Similar but smaller (~ 6 cm⁻¹) shifts are observed and modeled for the ν_4 PO₄ band at ~ 560 cm⁻¹.

In contrast, the spectroscopic properties of collagen-rich modern bone samples are better reproduced considering a binary composite containing 40 vol% of apatite particles and a second component with a dielectric constant $\epsilon_h = 2.5$, consistent with the dielectric properties of a collagen matrix (Wang et al. 1996). Compared with an apatite-air composite and for intermediate volume fractions, the increase in dielectric constant of the matrix leads to a prominent asymmetry of the ν_4 and ν_3 PO₄ bands in the diamond-ATR spectrum but only weakly affects the line shape of the Ge-ATR spectrum (Supplemental¹ Information), which is consistent with the experimental observations. This pertains to the stronger effects due to anomalous dispersion in the case of a reflection on an ATR crystal with lower refractive index such as diamond (Boulet-Audet et al. 2010). The low-frequency asymmetry of the ν_4 PO₄ band in the diamond ATR spectrum is particularly sensitive to the dielectric properties of the embedding matrix (Fig. 1). Note that their overlap with the broad and intense ν_3 PO₄ band results in an asymmetric line shape of the weak ν_2 CO₃ and ν_1 PO₄ bands in the diamond-ATR spectrum, a feature reproduced in the modeled spectrum. The spectra of HAR and BZ-PJ1-09 samples with intermediate amounts of collagen are close to those of modern ox bone. The properties of sample HAR, the estimated collagen content of which is ~ 16 wt%, are well reproduced using the same mineral fraction and matrix dielectric constant (ϵ_h) as for the modern bone. For the more transformed sample BZ-PJ1-09, the estimated collagen content (~ 11 wt%) of which is about half that of a modern bone, a better agreement with the experimental spectra is achieved for a lower value of the dielectric constant of the host matrix ($\epsilon_h = 1.9$), keeping the mineral fraction constant (40 vol%). The decrease in collagen content is correlated to a less pronounced broadening of the ν_3

PO₄ and ν₄ PO₄ diamond-ATR bands toward lower frequencies, reproduced in the model by lowering the dielectric constant of the host matrix.

In agreement with experimental observations, variations of ε_h result in little changes in the line shape of modeled Ge ATR spectra (Supplemental¹ Information). However, the theoretical spectra of collagen-rich samples overestimate the intensity of their experimental counterparts, which are about four times less intense than those of collagen-poor samples (e.g., for modern ox bone the theoretical intensities require a 0.175 scale factor to match the experimental ones). As discussed in Aufort et al. (2016), this theoretical overestimation is most likely related to sample heterogeneities, but further grinding of the collagen-rich samples did not allow recovering the theoretical intensities. Note that a decrease in the mineral fraction modifies the line shape (Supplemental Information) and cannot account for a simple decrease of the whole spectrum intensity.

Summarizing the present results, an effective medium modeling of the powder sample's dielectric properties based on the Bruggeman scheme and using a minimum number of free parameters accounts for the variability of major phosphate bands in the ATR spectrum of bone and tooth enamel samples with various collagen contents. Importantly, the microscopic properties of the apatite are not used as free parameters in the modeling of the different spectra, underlining the key influence of effective medium parameters. This further suggests that the strong ATR-FTIR bands related to phosphate vibrations are significantly affected by electrostatic effects occurring at a mesoscopic scale in the composite samples and much less by molecular-level interactions between the organic and inorganic components. Owing to these electrostatic effects, the experimental ATR-FTIR spectrum of a bone cannot be considered as a simple superposition of the ATR-FTIR spectra of apatite and collagen.

IMPLICATIONS

The study of bone material using ATR-FTIR spectroscopy is carried out in a broad range of fields, from paleontology, archaeology, and forensics to biomedical applications. Our results highlight yet another consequence of the complex composite nature of bone and of the intricate relationship between the closely intertwined organic and inorganic components at the different scales of bone's hierarchical structure. From the preservation assessment of archaeological finds to the conception of hydroxylapatite-based biomaterials for biomedical applications, the interpretation of ATR-FTIR spectra of bone materials should carefully consider mesoscopic-scale effects in addition to the atomic-scale organization of the sample.

ACKNOWLEDGMENTS

This work was supported by French state funds within the framework of the Cluster of Excellence MATISSE led by Sorbonne Universités and within the INTERRIVIE action of the 2016 CNRS-INSU TelluS program. We acknowledge support by the Sorbonne Universités FormInnov SPIREM project. We thank two anonymous reviewers and Robert B. Heimann for their thoughtful comments.

REFERENCES CITED

Aufort, J., Ségalen, L., Gervais, C., Brouder, C., and Balan, E. (2016) Modeling the attenuated total reflectance infrared (ATR-FTIR) spectrum of apatite. *Physics and Chemistry of Minerals*, 43, 615–626.

- Balan, E., Delattre, S., Roche, D., Segalen, L., Morin, G., Guillaumet, M., Blanchard, M., Lazzeri, M., Brouder, C., and Salje, E.K.H. (2011) Line-broadening effects in the powder infrared spectrum of apatite. *Physics and Chemistry of Minerals*, 38, 111–122.
- Beasley, M.M., Bartelink, E.J., Taylor, L., and Miller, R.M. (2014) Comparison of transmission FTIR, ATR, and DRIFT spectra: implications for assessment of bone bioapatite diagenesis. *Journal of Archaeological Science*, 46, 16–22.
- Boulet-Audet, M., Buffeteau, T., Boudreault, S., Daugey, N., and Pézolet, M. (2010) Quantitative determination of band distortions in diamond attenuated total reflectance infrared spectra. *Journal of Physical Chemistry B*, 114, 8255–8261.
- Bruggeman, D.A.G. (1935) Berechnung verschiedener physikalischer Konstanten von heterogenen Substanzen. I. Dielektrizitätskonstanten und Leitfähigkeiten der Mischkörper aus isotropen Substanzen. *Annalen der Physik*, 416, 665–679.
- Elliott, J.C. (2002) Calcium phosphate biominerals. In M.J. Kohn, J. Rakovan, and J.M. Hughes, Eds., *Phosphates: Geochemical, Geobiological, and Material Importance*, 48, p. 427–454. Reviews in Mineralogy and Geochemistry, Mineralogical Society of America, Chantilly, Virginia.
- Glimcher, M.J. (2006) Bone: Nature of the calcium phosphate crystals and cellular, structural, and physical chemical mechanisms in their formation. In N. Sahai and M.A.A. Schoonen, Eds., *Medical Mineralogy and Geochemistry*, 64, p. 223–282. Reviews in Mineralogy and Geochemistry, Mineralogical Society of America, Chantilly, Virginia.
- Hedges, R.E.M. (2002) Bone diagenesis: an overview of processes. *Archaeometry*, 44, 319–328.
- Iglesias, J.E., Ocana, M., and Serna, C.J. (1990) Aggregation and matrix effects on the infrared spectrum of microcrystalline powders. *Applied Spectroscopy*, 44, 418–426.
- Kendrick, J., and Burnett, A.D. (2016) PDIElec: The calculation of infrared and terahertz absorption for powdered crystals. *Journal of Computational Chemistry*, 37, 1491–1504. DOI: 10.1002/jcc.24344.
- Lebon M., Reiche I., Gallet X., Bellot-Gurlet., and Zazzo, A. (2016) Rapid quantification of bone collagen content by ATR-FTIR spectroscopy. *Radiocarbon*, 58, 131–145.
- LeGeros R.Z., and LeGeros J.P. (1984) Phosphate minerals in human tissue. In J.O. Nriagu, and P.B. Moore, Eds., *Phosphate Minerals*, p. 351–395. Springer-Verlag.
- Li, Z., and Pasteris, J.D. (2014) Chemistry of bone mineral, based on the hypermineralized rostrum of the beaked whale *Mesoplodon densirostris*. *American Mineralogist*, 99, 645–653.
- Pasteris, J.D., Wopenka, B., and Valsami-Jones, E. (2008) Bone and tooth mineralization: why apatite? *Elements*, 4, 97–104.
- Roche D., Ségalen L., Balan E., and Delattre S. (2010) Preservation assessment of Miocene-Pliocene tooth enamel from Tugen Hills (Kenyan Rift Valley) through FTIR, chemical and stable-isotope analyses. *Journal of Archaeological Science*, 37, 1690–1699.
- Skinner, H.C.W. (2005) Biominerals. *Mineralogical Magazine*, 69, 621–641.
- Snoeck, C., and Pellegrini, M. (2015) Comparing bioapatite carbonate pre-treatments for isotopic measurements: Part 1—Impact on structure and chemical composition. *Chemical Geology*, 417, 394–403.
- Stathopoulou, E.T., Psycharis, V., Chryssikos, G.D., Gionis, V., and Theodorou, G. (2008) Bone diagenesis: New data from infrared spectroscopy and X-ray diffraction. *Palaeogeography, Palaeoclimatology, Palaeoecology*, 266, 168–174.
- Surmik, D., Boczarowski, A., Balin, K., Dulski, M., Szade, J., Kremer, B., and Pawlicki, R. (2016) Spectroscopic studies on organic matter from Triassic reptile bones, Upper Silesia, Poland. *PLoS ONE*, 11(3), e0151143.
- Thompson, T.J.U., Gauthier, M., and Islam, M. (2009) The application of a new method of Fourier Transform Infrared Spectroscopy to the analysis of burned bone. *Journal of Archaeological Science*, 36, 910–914.
- Trueman, C.N., Privat, K., and Field, J. (2008) Why do crystallinity values fail to predict the extent of diagenetic alteration of bone mineral? *Palaeogeography, Palaeoclimatology, Palaeoecology*, 266, 160–167.
- Wang, X.J., Milner, T.E., Chang, M.C., and Nelson, J.S. (1996) Group refractive index measurement of dry and hydrated type I collagen films using optical low-coherence reflectometry. *Journal of Biomedical Optics*, 1, 212–216.
- Yi, H., Balan, E., Gervais, C., Segalen, L., Roche, D., Fayon, F., Person, A., Morin, G., and Babonneau, F. (2014) Probing atomic scale transformation of fossil enamel using FTIR and NMR spectroscopy: A case study from the Tugen Hills (Rift Gregory, Kenya). *Acta Biomaterialia*, 10, 3952–3958.

MANUSCRIPT RECEIVED SEPTEMBER 29, 2017

MANUSCRIPT ACCEPTED NOVEMBER 7, 2017

MANUSCRIPT HANDLED BY IAN SWAINSON

Endnote:

¹Deposit item AM-18-26320, Supplemental Material. Deposit items are free to all readers and found on the MSA web site, via the specific issue's Table of Contents (go to http://www.minsocam.org/MSA/AmMin/TOC/2018/Feb2018_data/Feb2018_data.html).